Turkish Journal of Electrical Engineering & Computer Sciences

http://journals.tubitak.gov.tr/elektrik/

Research Article

Turk J Elec Eng & Comp Sci
(2020) 28: 1612 – 1630

doi:10.3906/elk-1909-73

Nonlinear adaptive semiactive control of a half-vehicle model via hardware in the loop simulation

Mahmut PAKSOY, Muzaffer METİN*
Department of Mechanical Engineering, Yıldız Technical University, İstanbul, Turkey

Received: 13.09.2019 • **Accepted/Published Online:** 28.01.2020 • **Final Version:** 08.05.2020

Abstract: In this study, vehicle body vibrations are semiactively controlled using a nonlinear adaptive controller designed to improve passenger comfort by guaranteeing closed loop system stability under variable road disturbances with parametric uncertainty. Semiactive vibration control is implemented to the system through the magnetorheological damper. The MR damper test system is established in laboratory conditions, and the required values that are measured from the test system are used in computer simulations via the hardware in the loop simulation (HILS) method. By this way, it is possible to avoid the financial and other difficulties of the experimental study by establishing the test system completely, and also the hesitations that may arise in terms of producing realistic results of pure simulation studies of nonlinear dynamics. A 4-degree-of-freedom half-vehicle model is developed to examine the vehicle body bounce and pitch movements, and simulations are carried out under bump and random road irregularities, and the results are presented in comparison with the performance of the conventional skyhook controller. The performances of both controllers are interpreted from the aspect of acceleration and displacement responses of the vibrations and related criteria. As a result, the vibration reduction performances of both controllers are investigated experimentally using the HILS test system and the obtained results are evaluated with some comparative figures, performance criteria, and root mean square averages of vibrations.

Key words: Magnetorheological damper, hardware in the loop simulation, semiactive control, adaptive control, skyhook control

1. Introduction

Three types of suspension systems are used to increase passenger comfort in vehicles. These are passive, semiactive, and active suspension systems. They have advantages and disadvantages in comparison to each other. Passive suspension systems cannot provide the desired comfort level. On the other hand, active suspension systems are expensive systems and require large amounts of energy. However, because of their low energy requirements and satisfactory performance, semiactive suspension systems may also be preferred in vehicles.

In order to increase comfort in vehicles, the vibration reduction performance of suspension systems can be examined experimentally and/or theoretically [1, 2]. Although an experimental study provides reliable results, it generally takes a long time and a high cost to set up a fully experimental test rig. On the other hand, while a theoretical simulation study can produce results close to the real situation, it cannot precisely reflect a real result. To overcome these limitations the hardware in the loop simulation (HILS) method, which includes

*Correspondence: mmetin@yildiz.edu.tr

both experimental and theoretical parts, is proposed. The main idea of the HILS method; especially nonlinear systems, which are difficult to model mathematically, are experimentally created in the laboratory environment and fed online measured data into the numerical simulations.

The major advantage of the HILS method is the ability to create different operating conditions that can closely reflect real situations in the laboratory environment. Different semiactive suspension devices (MR damper, electro-rheological (ER) damper, etc.) can be tested in different road conditions, for different types of vehicle models using different parameters (mass, damping, stiffness, etc.). Therefore, the HILS method provides flexibility in studies. As a result, HILS is still a simulation of a real system with some of the subsystems included as simulated models and the rest being physically present. This makes the HILS study as accurate as its simulated parts. There are successful studies in the literature for this subject. Hwang et al. used a CVD (continuous variable damper) damper for semiactive control of a quarter vehicle model and they experimentally examined the results using the HILS method [3]. Choi et al. adapted the sliding mode control algorithm to a semiactive suspension system with an ER damper to reduce vertical vibrations by using the HILS method [4]. Lee and Choi suppressed the vibrations of a full vehicle model via an MR damper controlled by the skyhook method. They mounted only the left front suspension of the full vehicle model to the experimental HILS test system. They assumed that the other suspensions of the full vehicle had the same properties [5]. Choi et al. studied semiactive H∞ control performance of a full vehicle suspension system [6, 7]. Hong et al. designed a road-adaptive skyhook controller for a suspension system with a MacPherson type hydraulic strut. They used the HILS experimental method to investigate the vibration reduction performance of the skyhook controller [8]. Batterbee and Sims designed a HILS test system for a quarter vehicle model with an MR damper. They tested the skyhook and the feedback linearization control methods with a real road profile. They evaluated the results according to the related stability and comfort criteria [9]. Metered et al. designed a control method for suppressing a quarter-vehicle model's vibrations using artificial neural networks with an MR damper. Using the modified Bouc-Wen mathematical model and the HILS experimental test system, they investigated the results both numerically and experimentally [10]. Martinez et al. examined a quarter vehicle model with the HILS method developed as a hydraulic test system. They designed an FEB (frequency-estimation-based) controller for MR damper operations [11].

Parameters of a vehicle can be changed due to the number of passengers or heating of the dampers or springs. These uncertainties affect the designed control performance. Therefore, the designed controller must be able to overcome the parametric uncertainties. At this point, the adaptive control approach can give better performance for uncertain systems. Yıldız et al. [12] designed a nonlinear adaptive controller and H∞ controller for a quarter vehicle under parametric uncertainties. In their study, a ball screw mechanism was used for parameters identification of MR damper mathematical model. Effectiveness of the adaptive controller under parametric uncertainties was shown using some simulations and figures. Pang et al. [13] designed a nonlinear adaptive tracking controller using the backstepping approach for a half vehicle model which included uncertainties. Performance of their proposed approach was evaluated using some MATLAB-Simulink simulations under different road conditions. Song et al. [14] developed a semiactive nonlinear adaptive control to suppress passenger seat vibrations. In this design, it was assumed that the source of vibrations was unknown or unmeasurable and the system had parametric uncertainties. The success of their developed controller was examined by means of some simulations. Huang et al. [15] proposed a new adaptive law for parametric uncertainties of half vehicle which had active suspension systems. Effectiveness of their proposed adaptive control approach was investigated using only numerical simulations.

When the literature is examined, it can be said that the experimental studies related to the half vehicle model vibrations are limited because it can be difficult and costly to set up a complete test rig for the half vehicle model. In [4–7], the full vehicle model is studied experimentally but only one suspension is established in laboratory conditions and the other suspensions are fed from the same data, not independently operated. This approach is criticized in [10], where it is indicated that each suspension should be set up experimentally separately and, if each suspension is not built separately, then the study cannot be considered an experimental HIL simulation study. Therefore, two suspensions of half-vehicle are constructed separately for this experimental study. In [8, 9], the quarter vehicle model is examined by the HILS method and the adaptive control method is not used. In addition, in [8], the CVD damper is used in place of MR damper.

In this study, two different controllers (nonlinear adaptive and skyhook) are designed for vibration suppression of a half vehicle model and the results are compared to passive responses. The MR damper is used as a semiactive control element, and the system is designed as a HILS system in the laboratory. In addition, in the half-vehicle model, two suspensions are built completely apart. Finally, this study contributes to the literature in terms of experimental investigation of the half-vehicle model and the use of an adaptive control method for suppressing half vehicle vibrations.

2. Description of the HILS setup

The HILS method consists of both software and hardware components. The software section includes the mathematical model of the half vehicle, the control algorithm, and the MATLAB-Simulink software. Moreover, the hardware section consists of a dSPACE DS1103 control board, power supplies, and two ball-screw mechanisms with 10 mm lead (Figure 1). The first and second ball-screw mechanisms perform the relative displacement of the front and rear suspension systems, respectively. The first ball-screw mechanism consists of a 5 kW 3000 rpm servomotor, the Micro Epsilon optoNCDT 1700-100 laser displacement sensor, the Brüel & Kjaer 8230-002 force sensor and the RD-8041-1 long stroke MR damper. The second ball-screw mechanism consists of an 11 kW 3000 rpm servomotor, the AMETEK Solartron LVDT displacement sensor, the DYTRAN 1051V6 force sensor, and the RD-8041-1 long stroke MR damper. The numbered list of system components in Figure 1 is given in Table 1. The first ball-screw mechanism is specially constructed for this study. To reduce the cost, the study is also carried out using some of the existing laboratory facilities. The second ball-screw mechanism was already in our laboratory and it is just modified for this study.

Table 1. Component list of HILS setup.

Number of components	Definition	Number of components	Definition
1	Servomotor	8	MR damper
2	Coupling	9	Ball-screw mechanism
3	Force transducer	10	Wonder boxes
4	MR damper	11	Servomotor driver
5	Laser displacement sensor	12	dSPACE DS1103
6	Force transducer	13	Signal conditioner
7	LVDT	14	Power supplies

The purpose of the test system is to realize the relative displacement and velocity of the suspension system. Therefore, the relative displacement and velocity of the front and rear suspension system is obtained

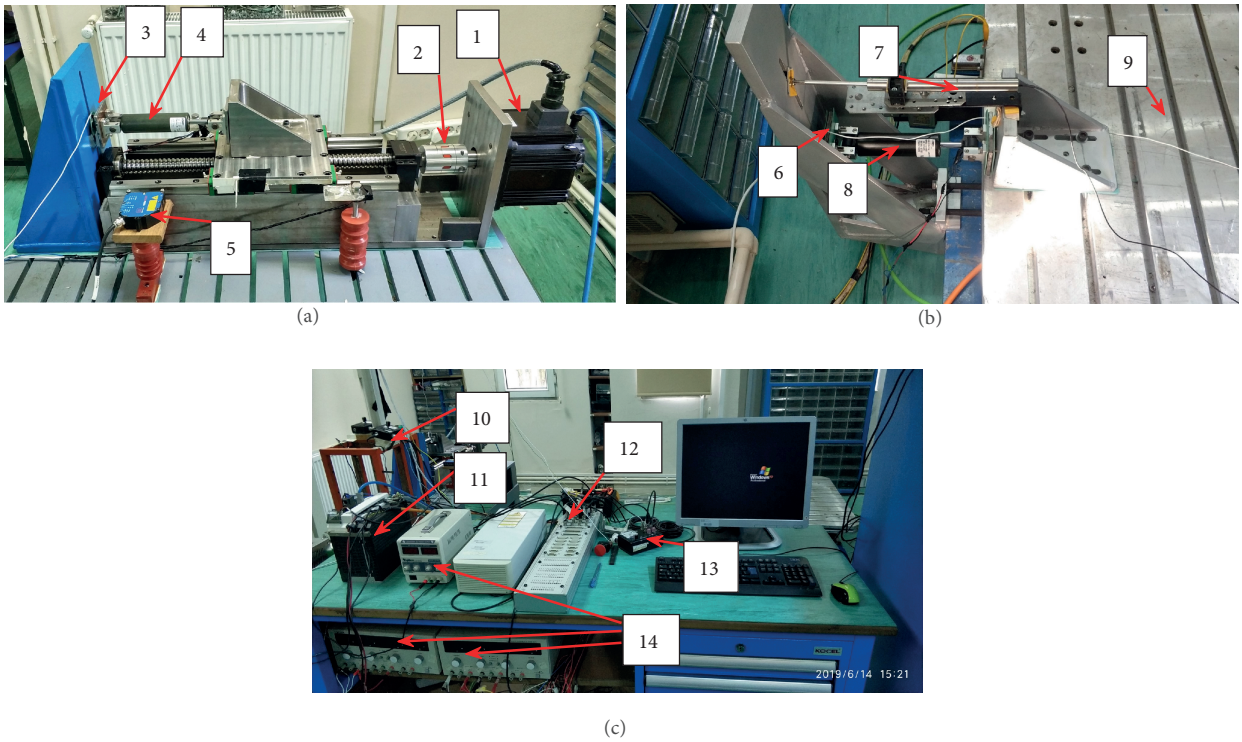

Figure 1. Experimental system (a) first ball-screw mechanism, (b) second ball screw mechanism, (c) other components.

from the dynamic equations of the half-vehicle model using the ball screw mechanism driven by the servomotors. To achieve the desired relative velocity experimentally, the servomotors are set to a ± 10 V analog speed mode. The laser and LVDT displacement sensors measure the relative displacement of the experimental system. Force sensors measure the damping force of the MR dampers, and these measured force data are fed into the dynamic model simulation on the computer. The desired velocities of the servomotors calculated by the MATLAB-Simulink program are transmitted to the servomotor drive via the dSPACE control board after being converted to voltage. The measured displacement data and the force sensor data are fed back to the simulation via the dSPACE control board. The operating mechanism of the experimental system is depicted schematically in Figure 2.

A reference signal with an amplitude of 10 mm and a frequency of 1 Hz is sent to the system to check if the test system correctly performed the desired displacement. In Figure 3a it can be seen that the HILS system could perform the desired displacement with time delay. In the HILS, time delay means that the system does not have correct speed or position at the desired time. In Figure 3b, v_ms and v_ds are the speed measured from servomotor encoder and the desired speed at 1 s, respectively. Thus, $v_ds - v_ms$ can be defined as error (e_rr). In order to compensate the time delay effect, the error must be zero. For this aim a PID controller is designed. The structure of the PID controller can be seen in Figure 3c.

3. Lugre mathematical model of MR damper

The physical models, working principles and application areas of MR dampers were described in previous studies [16, 17]. Besides, several models (Bingham model, Bouc-Wen model, Lugre model, etc.) have been developed

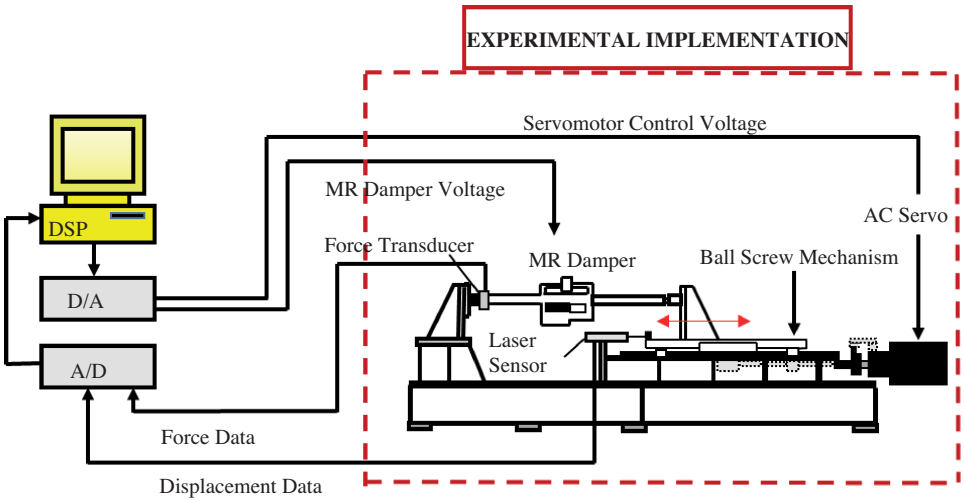

Figure 2. HILS schematic diagram.

to describe the hysteresis behavior of MR dampers in the literature [18]. Mathematical model of MR damper is required for adaptive controller design. In this study, the Lugre mathematical model is preferred because of its simple structure and satisfactory performance [19]. The mathematical equations of the Lugre model are defined as follows:

$$f_{mr} = \sigma_a z + \sigma_0 z v + \sigma_1 \dot{z} + \sigma_2 \dot{x} + \sigma_b \dot{x} v \tag{1}$$

$$\dot{z} = \dot{x} - a_0 \left|\dot{x}\right| z \tag{2}$$

where f_{mr} is damping force of the MR damper, $\dot{x}$ is the relative velocity of the MR damper, v is the applied voltage to the MR damper, z is the internal state variable related to the deformation of the MR fluid, and $\sigma_a, \sigma_0, \sigma_1, \sigma_2, \sigma_b, a_0$ are the constants used to define the hysteresis character of the MR damper. The values of the parameters used in the Lugre model are given in Table 2. As mentioned before, the Lugre model is used to design the adaptive controller because it is close to the actual system response. For this purpose, relative sinusoidal displacement which has 5 mm amplitude and 2 Hz frequency is applied to both the simulation and the experimental system, and MR damper damping forces are compared. Figure 4 shows that the numerical results obtained from the Lugre mathematical model are close to the experimental force sensor data.

Table 2. Lugre model parameters used in simulation [20].

Parameters	Values	Parameters	Values	Parameters	Values
σ_a	76,000 N/m	σ_2	1153.3 Ns/m	σ_1	3.21 Ns/m
σ_0	320,000 N/(mV)	σ_b	315 Ns/(mV)	a_0	1400 1/m

4. The half-vehicle model

The physical model of the half vehicle is shown in Figure 5. This model has four degrees of freedom, which are x_1, x_2, x_3 and θ. These are vertical motions of the vehicle body, front and rear wheels, and the pitch

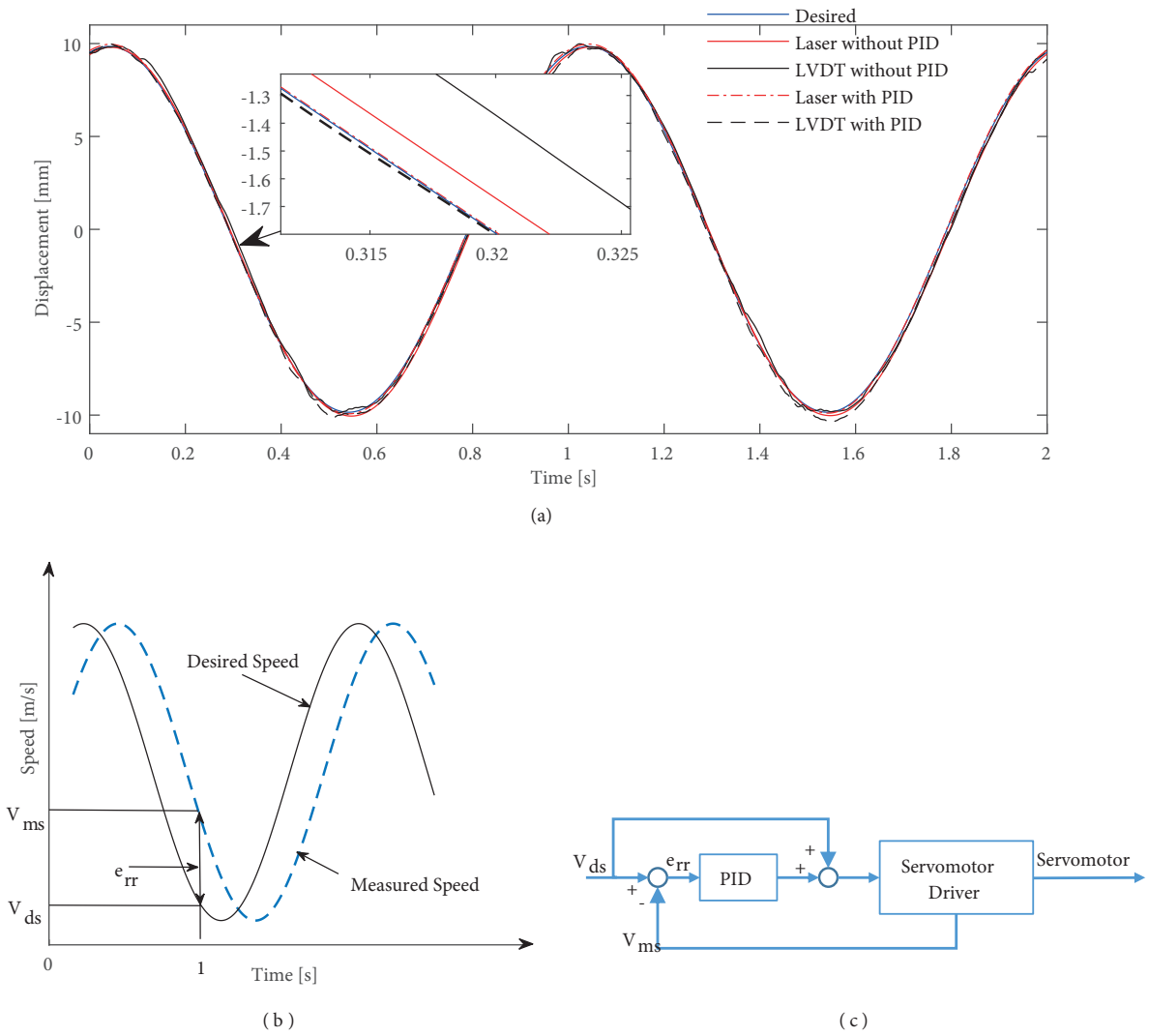

Figure 3. (a) Measured relative displacements from sensors, (b) identification of error for PID controller, (c) designed PID controller for delay compensation.

motion of the vehicle body, respectively. The model consists of a body and two wheels, these are joined with two suspension systems. m_1, m_2, and m_3 represent the vehicle body and front-rear wheelset masses, respectively. k_1 and k_2 are the linear spring stiffness values. The spring stiffness values of the vehicle's tires are indicated by k_t1 and k_t2. f_mr1 and f_mr2 are the damping force values of the MR dampers. The MR dampers that are used instead of passive dampers are positioned parallel to the suspension springs. In this study, MR dampers which are suitable for automotive applications and produced by LORD Corporation are used. Hence, MR dampers act as a conventional passive damper in the uncontrolled situation. Moreover, the conformity of MR damper characteristics with conventional passive damper characteristics is checked and MR damper selection is made accordingly.

The wheels are considered as linear spring elements that come into contact with the road. The damping coefficient of the wheels may be negligible because of their small values. The parameters of the half vehicle model are given in Table 3.

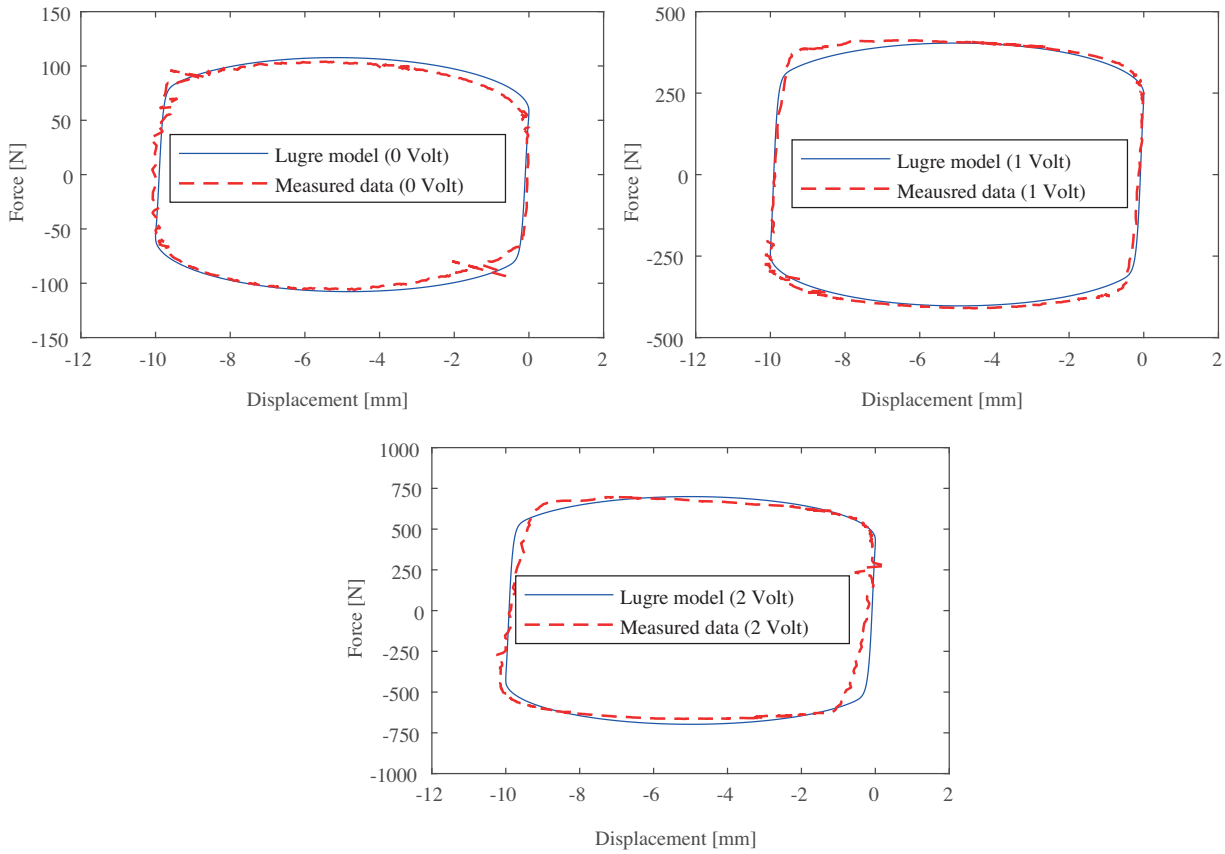

Figure 4. Comparison of experimental and simulation results of MR damper damping force.

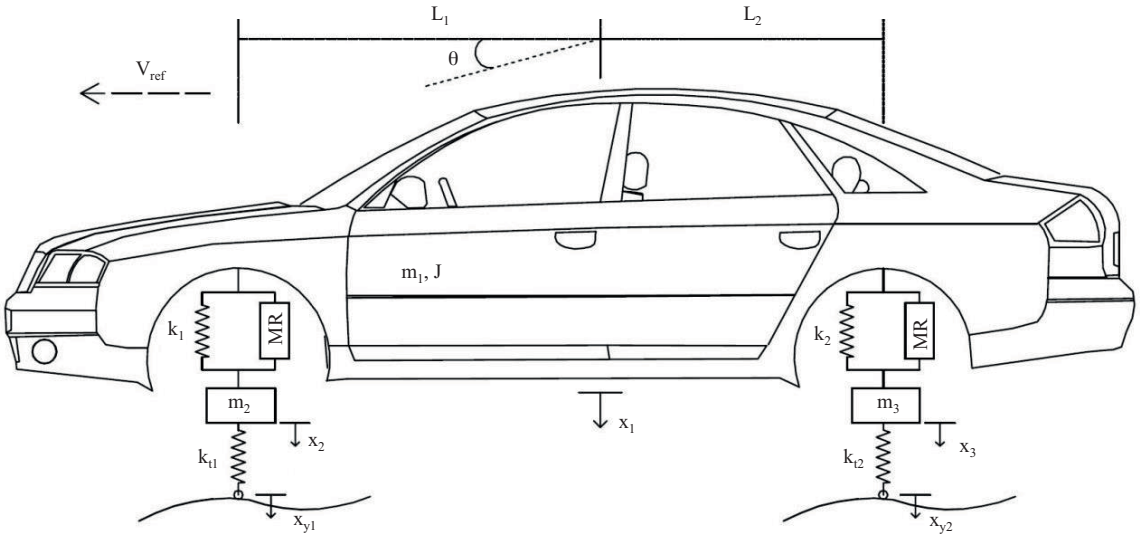

Figure 5. The half-vehicle model.

Table 3. Vehicle model parameters [21].

Parameters	Values	Parameters	Values	Parameters	Values
m_1	1180 kg	k_1	36,952 N/m	L_1	1.123 m
m_2	50 kg	k_2	30,130 N/m	L_2	1.377 m
m_3	45 kg	k_{t1}	140,000 N/m	k_{t2}	140,000 N/m
v_{ref}	10 m/s	J	633.615 kg m^2		

The differential equations of motion are written in matrix form as follows:

$$M\ddot{x}_s + K_s x_s + Hf + Ld = 0, \tag{3}$$

$$[M] = \begin{bmatrix} m_1 & 0 & 0 & 0 \\ 0 & J & 0 & 0 \\ 0 & 0 & m_2 & 0 \\ 0 & 0 & 0 & m_3 \end{bmatrix}, [K_s] = \begin{bmatrix} k_1 + k_2 & k_1L_1 - k_2L_2 & -k_1 & -k_2 \\ k_1L_1 - k_2L_2 & k_1{L_1}^2 + k_2{L_2}^2 & -k_1L_1 & k_2L_2 \\ -k_1 & -k_1L_1 & k_1 & 0 \\ -k_2 & k_2L_2 & 0 & k_2 \end{bmatrix}, [f] = \begin{bmatrix} f_{mr1} \\ f_{mr2} \end{bmatrix}, \tag{4}$$

$$[L] = \begin{bmatrix} 0 & 0 \\ 0 & 0 \\ -k_{t1} & 0 \\ 0 & -k_{t2} \end{bmatrix}, [d] = \begin{bmatrix} x_{y1} \\ x_{y2} \end{bmatrix}, [H] = \begin{bmatrix} 1 & 1 \\ L_1 & -L_2 \\ -1 & 0 \\ 0 & -1 \end{bmatrix}, [x_s] = \begin{bmatrix} x_1 & \theta & x_2 & x_3 \end{bmatrix}^T. \tag{5}$$

5. Skyhook controller design

The skyhook control method is often used to control semiactive systems because this method has a simple structure and good performance [5]. The classic skyhook control method works by switching between the maximum and minimum damping force values. Whether the maximum or minimum damping forces are applied to the system depends on the relative and upper-end point of the suspension. If the multiplication of the relative velocity with the velocity of the upper-end point of the suspension is positive, the maximum damping force is applied to the system; otherwise, minimum damping force is applied. Thus, in the skyhook control method, the desired damping force is defined as follows [22];

$$u_i = C_{sky}\dot{x}_{ui}\ , \qquad u_i = \begin{cases} u_{i\max} & \dot{x}_{ui}\left(\dot{x}_{ui} - \dot{x}_{bi}\right) > 0 \\ u_{i\min} & \dot{x}_{ui}\left(\dot{x}_{ui} - \dot{x}_{bi}\right) \le 0 \end{cases}, \qquad (i = 1, 2) \tag{6}$$

In equation (6), C_sky is control gain and u_i is desired damping force. $\dot{x}_ui$ is the velocity of the upper end of the suspension system and $\dot{x}_bi$ is the velocity of the bottom end point of the suspension system. In the magnetorheological (MR) mounted suspension system, the desired damping force u_i is the damping force of the MR damper (f_mri). Since the damping force of the MR damper varies according to the applied voltage, u_imax and u_imin can be selected as the maximum and minimum voltages of the MR damper, respectively. Hence, in the experiments, control voltages of the MR dampers are settled as 0V and 3V.

6. Semiactive nonlinear adaptive controller design

Equations of the Lugre model and the equations of motion in the form of matrices for the half vehicle model were previously given in equations (1)–(3), respectively. By combining equations (1) and (2), the MR damper forces are defined in matrix form as follows:

$$f_{mr} = \rho_1\theta_1 + \rho_2\theta_2, \tag{7}$$

where the auxiliary vector ρ_2 is a measurable parameter. ρ_1, θ_1, and θ_2 are the unknown parameters, so they should be estimated. The following equation is used to estimate the force of the MR damper:

$$\widehat{f}_{mr} = \widehat{\rho}_1\,\widehat{\theta}_1 + \rho_2\,\widehat{\theta}_2, \tag{8}$$

where $\widehat{\rho}_1$, $\widehat{\theta}_1$, and $\widehat{\theta}_2$ are the estimated values of the parameters.

6.1. Defining error dynamics

In the half-vehicle model, the displacement values must be zero to suppress the vibrations. If the error is defined as follows:

$$e = x_s - x_d \tag{9}$$

then x_d must be zero, because x_d is the desired displacement of the suspension. In this case the error dynamics e is equal to x_s, we define a new variable r to apply the error signal to the half vehicle model.

$$r = \dot{e} + \lambda e, \tag{10}$$

where λ is a constant, diagonal and positive definite gain matrix. The goal here is to make the variable $r(t)$ zero. For this purpose, the error dynamics are defined as follows:

$$M\dot{r} = \underbrace{M\lambda\dot{x}_s - K_s x_s - Ld}_{Y\phi} - Hf_m r, \tag{11}$$

where Y is the regression signal vector and ϕ is an unknown parameter vector. Y and ϕ are defined as follows:

$$Y = \begin{bmatrix} Ym & Yk \end{bmatrix}, \phi = \begin{bmatrix} \phi_m & \phi_k \end{bmatrix}^T \tag{12}$$

If $H\widehat{f}_{mr}$ is added to and subtracted from the equation (11), then the error dynamics can be written as follows:

$$M\dot{r} = Y\phi - Hf_{mr} + H\widehat{f}_{mr} - H\widehat{f}_{mr} \tag{13}$$

In order to avoid complexity in equations, χ, u_x, and Ω are defined as follows;

$$\chi = \begin{bmatrix} -\hat{\theta}^1_{11}\hat{z}_1 + \widehat{\theta}^{\,1}_{13}|\dot{x}_{mr1}|\,\widehat{z}_1 - \widehat{\theta}^{\,1}_{21}\dot{x}_{mr1} \\ -\hat{\theta}^2_{11}\hat{z}_2 + \widehat{\theta}^{\,2}_{13}|\dot{x}_{mr2}|\,\widehat{z}_2 - \widehat{\theta}^{\,2}_{21}\dot{x}_{mr2} \end{bmatrix}, \Omega = \begin{bmatrix} \hat{\theta}^1_{12}\hat{z}_1 + \widehat{\theta}^{\,1}_{22}\dot{x}_{mr1} & 0 \\ 0 & \hat{\theta}^2_{12}\hat{z}_2 + \widehat{\theta}^{\,2}_{22}\dot{x}_{mr2} \end{bmatrix}, u_x = \Omega v \tag{14}$$

In the next step, taking the stability analysis into account, the expression Hu_x is written as follows:

$$Hu_x = Kr + H\chi + Y\widehat{\phi} - H\zeta_a \widehat{\theta}_1^{\,1} - H\zeta_b \widehat{\theta}_1^{\,2} v + H\zeta_c \widehat{\theta}_1^{\,3}. \tag{15}$$

The voltage expression v that is voltage of the MR dampers can be obtained from equations (14) and (15) as equation (16).

$$v = H^{-1} \frac{Kr + H\chi + Y\widehat{\phi} - H\zeta_a \widehat{\theta}_1^{\,1} + H\zeta_c \widehat{\theta}_1^{\,3}}{\Omega + \zeta_b \widehat{\theta}_1^{\,2}}, \tag{16}$$

where

$$\hat{\theta}_1^1 = \begin{bmatrix} \hat{\theta}_{11}^1 \\ \hat{\theta}_{11}^2 \end{bmatrix}, \hat{\theta}_1^2 = \begin{bmatrix} \hat{\theta}_{12}^1 & 0 \\ 0 & \hat{\theta}_{12}^2 \end{bmatrix}, \hat{\theta}_1^3 = \begin{bmatrix} \hat{\theta}_{13}^1 |\dot{x}_{mr1}| \\ \hat{\theta}_{13}^2 |\dot{x}_{mr2}| \end{bmatrix}, \tag{17}$$

$$\zeta_a = \begin{bmatrix} \zeta_1 & 0 \\ 0 & \zeta_4 \end{bmatrix}, \zeta_b = \begin{bmatrix} \zeta_2 & 0 \\ 0 & \zeta_5 \end{bmatrix}, \zeta_c = \begin{bmatrix} \zeta_3 & 0 \\ 0 & \zeta_6 \end{bmatrix}. \tag{18}$$

In order to formulate the estimated force, we need an observer to observe the internal state $z(t)$ because $z(t)$ is internal state variable and unmeasurable via sensors. Based on the subsequent stability analysis and assuming that the parameter a_0 is positive, the following observer is designed for $z(t)$:

$$\dot{\tilde{z}} = -a_0 |\dot{x}_{mr}| \tilde{z} \tag{19}$$

In this step, the estimation errors of the parameters are written as;

$$\begin{array}{l} \tilde{z}_1 = z_1 - \hat{z}_1,\ \tilde{z}_2 = z_2 - \hat{z}_2,\ \tilde{\phi} = \phi - \hat{\phi},\ \tilde{\theta}_{21} = \theta_{21} - \hat{\theta}_{21} \\ \tilde{\theta}_{22} = \theta_{22} - \hat{\theta}_{22},\ \tilde{\theta}_{11} = \theta_{11} - \tilde{\theta}_{11},\ \tilde{\theta}_{12} = \theta_{12} - \tilde{\theta}_{12},\ \tilde{\theta}_{13} = \theta_{13} - \tilde{\theta}_{13} \end{array} \tag{20}$$

Using the parameter estimation errors, the expression $M\dot{r}$ can be written as follows:

$$\begin{array}{l} M\dot{r} = Y\tilde{\phi} - Kr - H\rho_2\tilde{\theta}_2 - H \begin{bmatrix} \tilde{\theta}_{11}^1(\tilde{z}_1 + \zeta_1) + \theta^1{}_{11}(\tilde{z}_1 - \zeta_1) \\ \tilde{\theta}_{11}^2(\tilde{z}_2 + \zeta_4) + \theta^2{}_{11}(\tilde{z}_2 - \zeta_4) \end{bmatrix} \\ -H \begin{bmatrix} \tilde{\theta}_{12}^1(\tilde{z}_1 + \zeta_2)v_1 + \theta^1{}_{12}(\tilde{z}_1 - \zeta_2)v_1 \\ \tilde{\theta}_{12}^2(\tilde{z}_2 + \zeta_5)v_2 + \theta^2{}_{12}(\tilde{z}_2 - \zeta_5)v_2 \end{bmatrix} + H \begin{bmatrix} \tilde{\theta}_{13}^1 |\dot{x}_{mr1}| (\tilde{z}_1 + \zeta_3) + \theta^1{}_{13} |\dot{x}_{mr1}| (\tilde{z}_1 - \zeta_3) \\ \tilde{\theta}_{13}^2 |\dot{x}_{mr2}| (\tilde{z}_2 + \zeta_6) + \theta^1{}_{13} |\dot{x}_{mr2}| (\tilde{z}_2 - \zeta_6) \end{bmatrix} \end{array} \tag{21}$$

where $\xi_1, \xi_2, \xi_3, \xi_4, \xi_5, \xi_6$ are the auxiliary filters. The auxiliary filters are defined in the equation (23).

6.2. Stability analysis

For the stability analysis, a candidate positive definite Lyapunov function should be selected. The candidate Lyapunov function "V" is selected as follows;

$$\begin{array}{l} V = \frac{1}{2} r^T M r + \frac{1}{2}\tilde{z}_1^2 + \frac{1}{2}\tilde{z}_2^2 + \frac{1}{2}\tilde{\phi}^T \Gamma_\phi^{-1} \tilde{\phi} + \frac{1}{2}\tilde{\theta}_2^T \Gamma_2^{-1} \tilde{\theta}_2 + \frac{1}{2}\frac{1}{\gamma_1}\tilde{\theta}_1^1 1^2 + \frac{1}{2}\frac{1}{\gamma_2}\tilde{\theta}_1^1 2^2 + \frac{1}{2}\frac{1}{\gamma_3}\tilde{\theta}_{13}^{1\,2} + \frac{1}{2}\tilde{\theta}_{11}^1(\tilde{z}_1 - \xi_1)^2 \\ + \frac{1}{2}\tilde{\theta}_{12}^1(\tilde{z}_1 - \xi_2)^2 + \frac{1}{2}\tilde{\theta}_{13}^1(\tilde{z}_1 - \xi_3)^2 + \frac{1}{2}\frac{1}{\gamma_4}\tilde{\theta}_{11}^{2^2} + \frac{1}{2}\frac{1}{\gamma_5}\tilde{\theta}_{12}^{2^2} + \frac{1}{2}\frac{1}{\gamma_6}\tilde{\theta}_{13}^{2^2} + \frac{1}{2}\tilde{\theta}_{11}^2(\tilde{z}_2 - \xi_4)^2 + \frac{1}{2}\tilde{\theta}_{12}^2(\tilde{z}_2 - \xi_5)^2 \\ + \frac{1}{2}\tilde{\theta}_{13}^2(\tilde{z}_2 - \xi_6)^2 \end{array}, \tag{22}$$

where Γ_ϕ, Γ_2 are the diagonal positive definite adaptation gain matrices, and γ_1, γ_2, and γ_3 are the positive adaptation gains. The adaptation rules are designed as in the equation (23).

$$\begin{array}{l}\dot{\hat{\phi}} = -\dot{\tilde{\phi}} = -\Gamma Y^T r \\ \dot{\hat{\theta}}_2 = \dot{\tilde{\theta}}_2 = \Gamma_2 \rho_2^T H^T r \\ \dot{\hat{\theta}}^1_{11} = -\dot{\tilde{\theta}}^1_{11} = \gamma_1(\hat{z}_1 + \xi_1)H^T r \\ \dot{\hat{\theta}}^2_{11} = -\dot{\tilde{\theta}}^2_{11} = \gamma_4(\hat{z}_2 + \xi_4)H^T r \\ \dot{\hat{\theta}}^1_{12} = -\dot{\tilde{\theta}}^1_{12} = \gamma_2 v_1(\hat{z}_1 + \xi_2)H^T r \\ \dot{\hat{\theta}}^2_{12} = -\dot{\tilde{\theta}}^2_{12} = \gamma_5 v_2(\hat{z}_2 + \xi_5)H^T r \\ \dot{\hat{\theta}}^1_{13} = -\dot{\tilde{\theta}}^1_{13} = -\gamma_3 \left|\dot{x}_{mr1}\right|(\hat{z}_1 + \xi_3)H^T r \\ \dot{\hat{\theta}}^2_{13} = -\dot{\tilde{\theta}}^2_{13} = -\gamma_6 \left|\dot{x}_{mr2}\right|(\hat{z}_2 + \xi_6)H^T r \end{array} , \quad \begin{array}{l}\dot{\xi}_1 = -a_0 \left|\dot{x}_{mr1}\right| \xi_1 - H^T r \\ \dot{\xi}_2 = -a_0 \left|\dot{x}_{mr1}\right| \xi_2 - v_1 H^T r \\ \dot{\xi}_3 = -a_0 \left|\dot{x}_{mr1}\right| \xi_3 + \left|\dot{x}_{mr1}\right| H^T r \\ \dot{\xi}_4 = -a_0 \left|\dot{x}_{mr2}\right| \xi_4 - H^T r \\ \dot{\xi}_5 = -a_0 \left|\dot{x}_{mr2}\right| \xi_5 - v_2 H^T r \\ \dot{\xi}_6 = -a_0 \left|\dot{x}_{mr2}\right| \xi_6 + \left|\dot{x}_{mr2}\right| H^T r \end{array} \tag{23}$$

Using the adaptation rules, the derivative of the Lyapunov function becomes the following:

$$\begin{array}{l}\dot{V} = -r^T K r - r^T H \left[\begin{array}{c}\theta^1_{11}(\widehat{z}_1 - \xi_1) \\ \theta^2_{11}(\widehat{z}_2 - \xi_4)\end{array}\right] - r^T H \left[\begin{array}{c}\theta^1_{12}(\widehat{z}_1 - \xi_2) \\ \theta^2_{12}(\widehat{z}_2 - \xi_5)\end{array}\right] + r^T H \left[\begin{array}{c}\theta^1_{13}\left|\dot{x}_{mr1}\right|(\widehat{z}_1 - \xi_3) \\ \theta^1_{13}\left|\dot{x}_{mr2}\right|(\widehat{z}_2 - \xi_6)\end{array}\right] \\ -a_0 \left|\dot{x}_{mr1}\right| \tilde{z}_1^2 - a_0 \left|\dot{x}_{mr2}\right| \tilde{z}_2^2 + \theta^1_{11}(\tilde{z}_1 - \xi_1)(\dot{\tilde{z}}_1 - \dot{\xi}_1) + \theta^2_{11}(\tilde{z}_2 - \xi_4)(\dot{\tilde{z}}_2 - \dot{\xi}_4) + \theta^1_{12}(\tilde{z}_1 - \xi_2)(\dot{\tilde{z}}_1 - \dot{\xi}_2) \\ +\theta^2_{12}(\tilde{z}_2 - \xi_5)(\dot{\tilde{z}}_2 - \dot{\xi}_5) + \theta^1_{13}(\tilde{z}_1 - \xi_3)(\dot{\tilde{z}}_1 - \dot{\xi}_3) + \theta^2_{13}(\tilde{z}_2 - \xi_6)(\dot{\tilde{z}}_2 - \dot{\xi}_6)\end{array} \tag{24}$$

The derivative of the Lyapunov function is obtained in the form (25) when the auxiliary filters are placed in the equations.

$$\begin{array}{l}\dot{V} = -r^T K r - a_0 \left|\dot{x}_{mr1}\right| \tilde{z}_1^2 - a_0 \left|\dot{x}_{mr2}\right| \tilde{z}_2^2 - a_0 \theta^1_{11} \left|\dot{x}_{mr1}\right| (\tilde{z}_1 - \xi_1)^2 - a_0 \theta^1_{12} \left|\dot{x}_{mr1}\right| (\tilde{z}_1 - \xi_2)^2 \\ -a_0 \theta^1_{13} \left|\dot{x}_{mr1}\right| (\tilde{z}_1 - \xi_3)^2 - a_0 \theta^2_{11} \left|\dot{x}_{mr2}\right| (\tilde{z}_2 - \xi_4)^2 - a_0 \theta^2_{12} \left|\dot{x}_{mr2}\right| (\tilde{z}_2 - \xi_5)^2 - a_0 \theta^2_{13} \left|\dot{x}_{mr2}\right| (\tilde{z}_2 - \xi_6)^2\end{array} \tag{25}$$

Here, the last eight terms are always negative, enabling us to find the upper bound as (26);

$$\dot{V} \leq -r^T K r \tag{26}$$

Therefore, if the control gain K is selected to be positive definite, it can be concluded that the derivative of the Lyapunov function is always negative. Hence, the system is stable.

7. Experimental results

The HILS test system is used to experimentally investigate nonlinear adaptive control and skyhook control performances for a half vehicle model. Here, two different road inputs are implemented (bump and random) to evaluate the performance of the controllers. The bump input is described in (27), and it is applied to the system by using a 1-s transport delay.

$$z_r(t) = \begin{cases} \frac{a}{2}\left[1 - \cos(\frac{2\pi v_0 t}{l})\right] & 0 \leq t \leq \frac{l}{v_0} \\ 0 & t > \frac{l}{v_0} \end{cases} \tag{27}$$

Additionally, the random road profile that is produced according to the ISO 8608 road classification is used in this study. The geometric irregularities of the road surface are ignored in the lateral direction and they

are considered to be the sum of the sinusoidal harmonic wave series. The roughness profile in terms of power spectral density (PSD) of the vertical displacements can be created from the following equation [23].

$$z_r(t) = 10^{-3} 2^k \Delta n^{-1/2} n_0 \sum_{i=1}^{N} \cos(2\pi i \Delta n t + \varphi i) \frac{1}{i}, \tag{28}$$

where k is the degree of road roughness as given in Table 4. Considering the ability of the servomotors, the road disturbance coefficient between A and B is accepted as $k = 3$, and the vehicle velocity is selected as 10 m/s. n_0 is the reference spatial frequency ($n_0 = 0.1$ cycles/m), N is the number of data points, Δn is the time interval between each discretized spatial frequency, and φi is a set of random phase angle values with a uniform distribution in the range $0 - 2\pi$. The generated road profile can be seen in Figure 6.

Table 4. ISO 8608 Road Classification [23]

Road class		k	Road class		k	Road class		k
Upper limit	Lower limit		Upper limit	Lower limit		Upper limit	Lower limit	
A	B	3	D	E	6	G	H	9
B	C	4	E	F	7			
C	D	5	F	G	8			

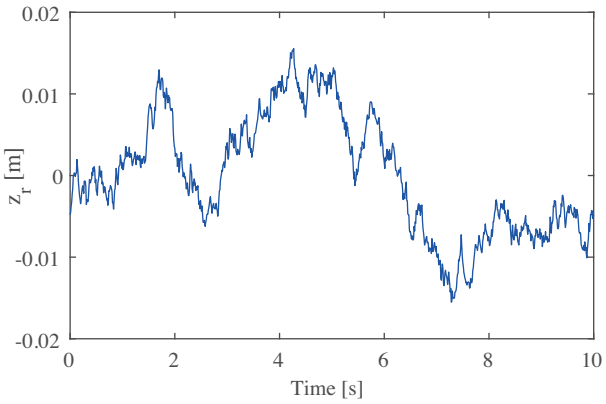

Figure 6. A-B class ISO 8608 road profile for the constant 10m/s velocity.

The relative velocity that is obtained according to the applied road input is calculated by the MATLAB-Simulink program and then fed to the servomotor drive with the dSPACE control board after the voltage conversion. The servomotors perform relative displacements via ball-screw mechanisms. The variable damping force data of the MR dampers which measured using force sensors are fed back to the simulation by means of dSPACE control board. Nonlinear adaptive and skyhook controllers are modeled using the MATLAB-Simulink program. The results are analyzed using both root mean square (RMS) values and performance criteria for both the controlled and uncontrolled situations. In the figures, straight, dashed, and dotted lines indicate passive, nonlinear adaptive, and skyhook control results, respectively.

7.1. Bump road case results

The relative displacement values of the front and rear suspensions are given in Figure 7. The time response of the relative displacements of the front and rear suspensions are more suppressed than the skyhook controller by the use of the adaptive controller. Figure 8 shows the vertical and angular accelerations of the vehicle body. In Figure 8, it can be seen that both controllers provide close results for the vertical acceleration of the vehicle body.

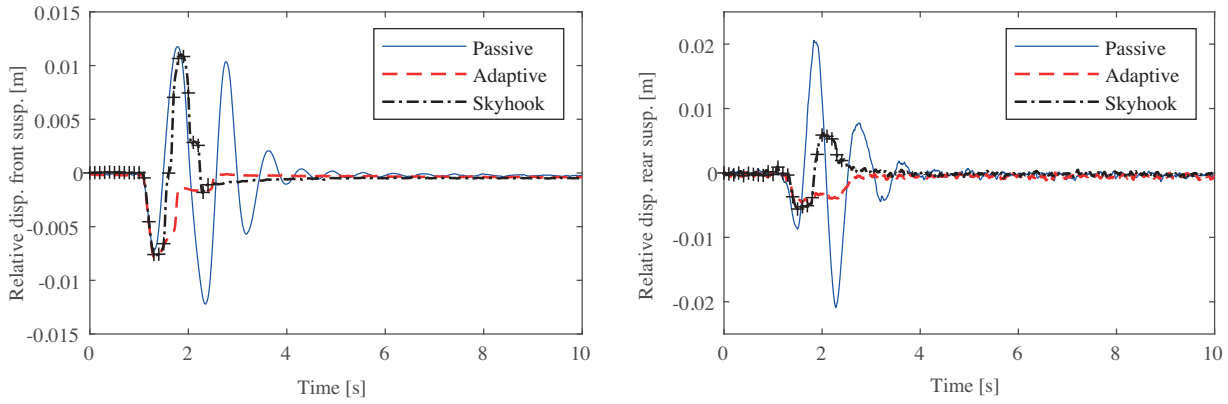

Figure 7. Relative displacements of front and rear suspensions.

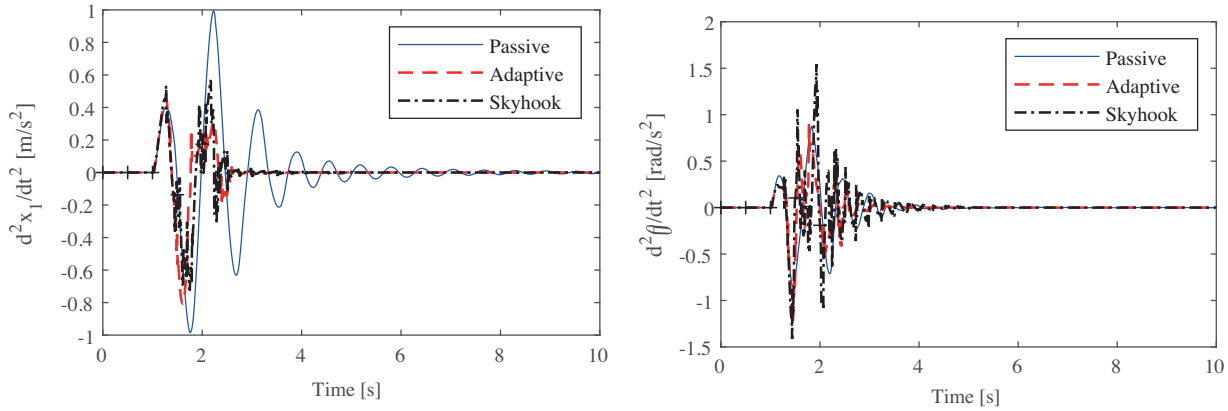

Figure 8. Vertical and angular accelerations of vehicle body.

7.2. ISO road case results

An ISO road profile input is applied to the vehicle, and the results are evaluated. In Figure 9 both controllers are between suspension stroke for the suspension travels. The acceleration responses are given in Figure 10. It is seen that the adaptive controller provides better results than the passive system, and the skyhook controller has deteriorated responses in comparison to the passive system.

7.3. Discussion

An automotive suspension system should support the following tasks: To suppress vibrations from road, to keep good road holding and handling on a rough and bumpy road, a winding road, or braking, and finally to

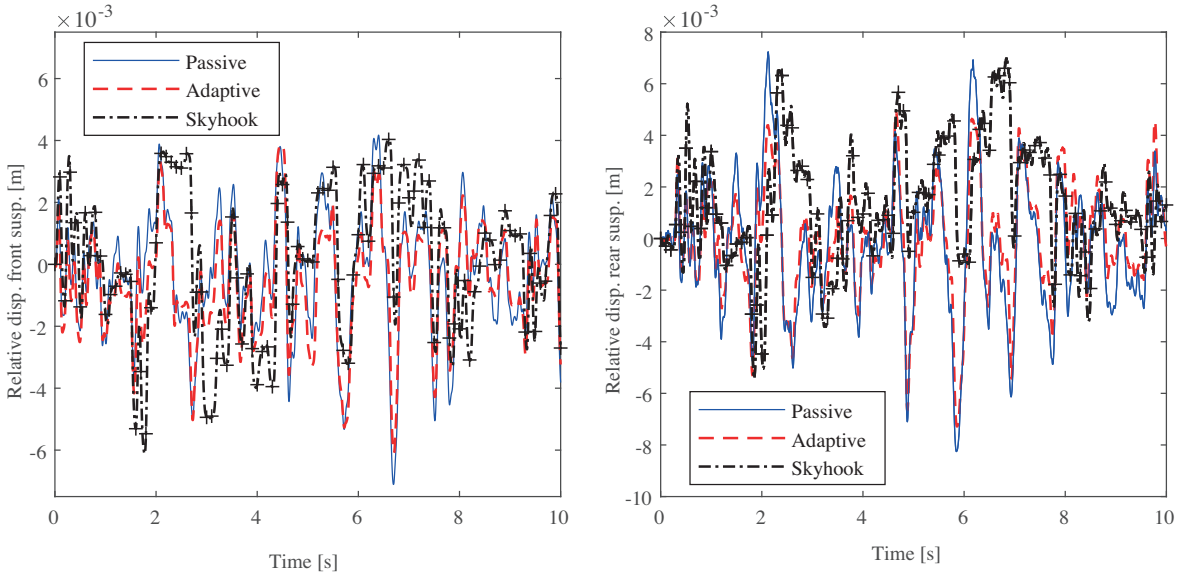

Figure 9. Relative displacements of front and rear suspensions under random excitation.

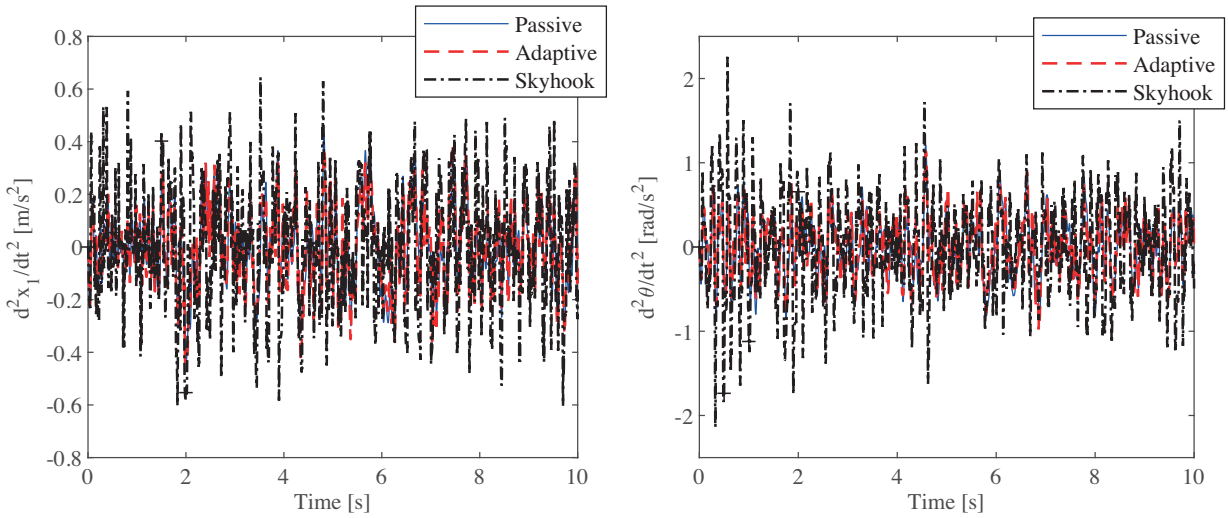

Figure 10. Vertical and angular accelerations of vehicle body under random excitation.

support the vehicle static weight. Based on this explanation, this paper aims to reduce vibrations to improve passenger comfort and ride quality. In general, ride quality can be measured by the vertical acceleration of the passenger's locations. Roll and pitch accelerations are not important to improve ride quality even though they are critical quantities for handling issues. On the other hand, ride quality is very subjective, the easiest quantity is road holding which is represented by the tire deflection. Road holding is easier to quantify and is related to the variations in the normal forces. Tire force variations are directly related to tire deflections, reducing tire deflection results in improved traction, braking. The vehicle's static weight can be measured by the suspension deflection and depends on the type of suspension used [24, 25]. In addition, while the controllers suppress vehicle vibrations, the limit stroke values in the suspension systems must not be exceeded. Therefore, the relative displacement of the suspension is an important parameter to be analyzed. For these aims, relative

displacements of suspensions, vertical and angular accelerations of the vehicle body, and dynamic tire loads are investigated in this study. Moreover, the voltage values applied to MR dampers are presented in the comparison of controller performances in terms of energy efficiency.

Vibration responses of the vehicle body are examined in terms of RMS averages to compare passive and semiactive cases (Table 5). The RMS averages are calculated by taking both types of road disturbances into account. Table 5 shows that both controllers are successful for the bump road input. When the ISO road input is applied to the system, the skyhook controller worsens the responses, but the adaptive controller successfully suppresses the vibrations. Additionally, the RMS values are evaluated as percentages as follows:

- In terms of vertical displacement of the vehicle body for the bump road input, the skyhook controller provides a 27% improvement in comparison to the passive system while the adaptive controller provides a 40% improvement,
- Both controllers achieve approximately 47% improvement in the vertical acceleration of the vehicle body,
- Considering the angular motion of the vehicle body, the skyhook and adaptive controllers improve the responses by 38% and 29%, respectively.
- When the angular acceleration of the vehicle body is evaluated, the adaptive controller provides approximately 10% improvement, while the skyhook controller causes a 13% deterioration in system responses.

When ISO road input is applied to the system, the results are as follows:

- The skyhook and adaptive controllers reduce the displacement of the vehicle body's vibrations by 12% and 6%, respectively,
- If the vertical acceleration of the vehicle body is examined, the skyhook controller causes a deterioration of 32%, while the adaptive controller achieves an improvement of 8%,
- While the adaptive controller provides 13% improvement, the skyhook controller reaches 45% in terms of the angular displacement of the vehicle body,
- While evaluating the angular acceleration of the vehicle body, the skyhook controller causes a 47% deterioration, while the adaptive controller provides an improvement of approximately 14%.

Table 5. Comparison of RMS averages.

Bump road input	x_1	$\ddot{x}_1$	θ	$\ddot{\theta}$	ISO road input	x_1	$\ddot{x}_1$	θ	$\ddot{\theta}$
Passive	0.0087	0.2460	0.0031	0.1889	Passive	0.0075	0.1512	0.0022	0.3565
Adaptive control	0.0052	0.1295	0.0022	0.1701	Adaptive control	0.0070	0.1390	0.0019	0.3082
Skyhook control	0.0063	0.1302	0.0019	0.2142	Skyhook control	0.0066	0.1996	0.0012	0.5264

For examining the performance of a controller, the methods of integral of the absolute error (IAE), integral of the time-multiplied absolute error (ITAE), integral of the squared error (ISE) and integral of time-multiplied squared error (ITSE) are preferred frequently. The performance indices' values that are obtained in this study are given in Table 6. Performance indices are often used to assess the success of reducing vibrations in control studies.

Table 6 shows the vertical and angular acceleration values of the vehicle body because accelerations are the most important parameters that affect driving comfort. According to Table 6, the adaptive controller

provides improvements of up to 79% and 25% in the accelerations of the vehicle body under bump and ISO road inputs compared to the passive situation, respectively. On the other hand, the skyhook controller achieves up to 77% improvement in vehicle body accelerations under bump road input, but cannot succeed to suppress the vibrations under ISO road input in terms of performances criteria comparison.

Table 6. Performance criteria values.

Bump road input								
Value	$\ddot{x}_1$				$\ddot{\theta}$			
	IAE	ITAE	ISE	ITSE	IAE	ITAE	ISE	ITSE
Passive	1.1233	2.7146	0.6053	1.2955	0.7221	1.4298	0.3550	0.6442
Adaptive control	0.4035	0.6815	0.1676	0.2692	0.5145	0.9227	0.2654	0.4370
%	%64	%74	%72	%79	%28	%35	%25	%32
Skyhook control	0.4260	0.7445	0.1696	0.2903	0.6769	1.3562	0.4117	0.7420
%	%62	%72	%72	%77	%6	%5	%15	%15
ISO road input								
Value	$\ddot{x}_1$				$\ddot{\theta}$			
	IAE	ITAE	ISE	ITSE	IAE	ITAE	ISE	ITSE
Passive	1.2108	6.0719	0.2287	1.1462	2.8856	14.1803	1.2709	6.0782
Adaptive control	1.1174	5.8257	0.1932	1.0139	2.5137	12.3822	0.9499	4.6320
%	%8	%4	%15	%12	%12	%12	%25	%23
Skyhook control	1.5827	8.0672	0.3982	2.0070	4.2661	19.7046	2.7710	11.5769
%	%-30	%-32	%-74	%-74	%-47	%-38	%-110	%-90

If equation 6 is examined, it can be seen that the skyhook controller has a simple structure and operates with maximum voltage (3 V) or minimum voltage (0 V) as on/off. Therefore, the skyhook controller can cause acceleration jumps under random road input due to its implementation principle [26].

Road holding can be assessed by examining dynamic tire loads. Therefore, dynamic tire loads of the half vehicle model are given to examine the road holding issue in Figures 11 and 12. If taking into consideration the vertical static tire loads, Figures 11 and 12 show that both controllers provide road holding while suppressing vibrations.

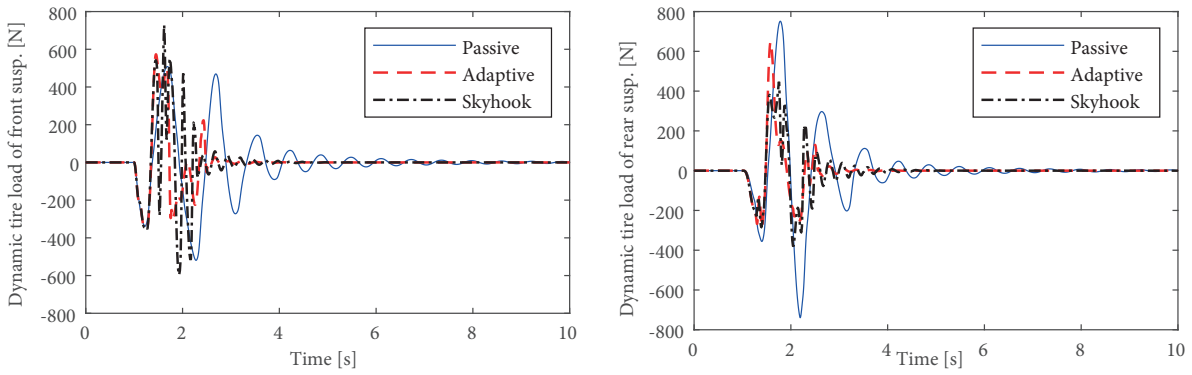

Figure 11. Dynamic tire load responses under bump excitation.

Figure 13 shows the voltage amount sent by the controllers to the MR dampers. As the skyhook controller only operates between the maximum and minimum values, it produces more intense voltage in comparison to the adaptive controller.

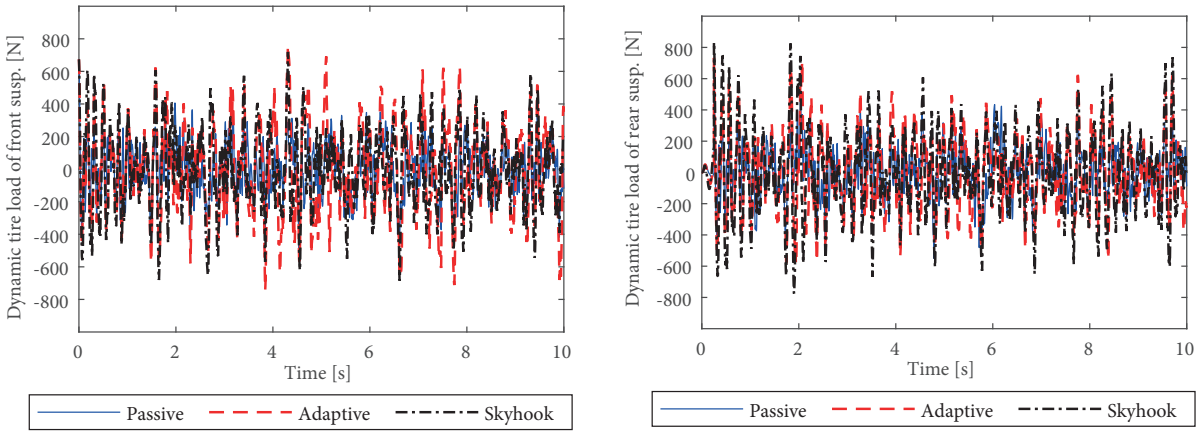

Figure 12. Dynamic tire load responses under random excitation.

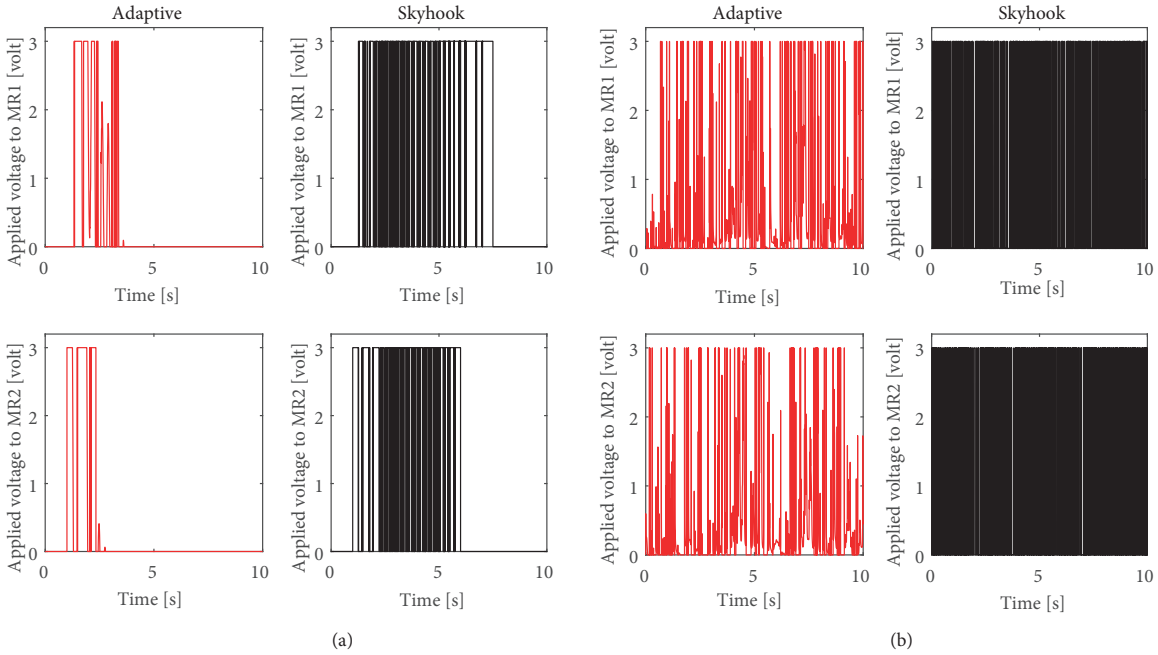

Figure 13. Applied voltages to MR dampers (a) under bump excitation (b) under random excitation.

8. Conclusions

With the HILS approach, a significant part of actual driving conditions can be experimentally constructed, and the measured data from the test system can be fed online to the simulation. Thus, more realistic results can be obtained with HILS than pure numerical simulation results. The HILS system combines both experimental hardware and theoretical simulation. Hardware components consist of MR dampers, ball screw mechanisms,

Servomotors, dSPACE control board, and force and displacement sensors. Dynamic analysis of the half vehicle model is performed via MATLAB-Simulink software. The two MR dampers are used as a semiactive suspension system to suppress vehicle body vibrations. The vehicle system is considered to have 4 degrees of freedom in the half vehicle model. Both bump and random road inputs are applied to the system as two different road disturbances. To suppress the vehicle vibrations, the MR dampers are controlled by skyhook and nonlinear adaptive as two different control algorithms. The results that are obtained by the control implementations are compared to passive system results. When the results are evaluated, it is seen that the most successful results in terms of suppressing vehicle vibrations under different road irregularities are achieved by the nonlinear adaptive control implementation. Furthermore, it is seen that the skyhook control algorithm does not produce successful acceleration reduction results under the influence of the ISO road disturbance input. In conclusion, adding an MR damper controlled with the nonlinear adaptive method to vehicle suspensions improves ride comfort, and the disturbances felt by the passengers are reduced. Expanding the proposed method with consideration of an adaptive time delay cancellation might be a direction for further studies.

References

[1] Ahmadian M, Pare CA. A quarter-car experimental analysis of alternative semiactive control methods. Journal of Intelligent Material Systems and Structures 2000; 11 (8): 604-612. doi: 10.1106/MR3W-5D8W-0LPL-WGUQ

[2] Paksoy M, Guclu R, Cetin S. Semiactive self-tuning fuzzy logic control of full vehicle model with MR damper. Advances in Mechanical Engineering 2014; 6: 816813. doi: 10.1155/2014/816813

[3] Hwang SH, Heo SJ, Kim HS, Lee KI. Vehicle dynamic analysis and evaluation of continuously controlled semi-active suspensions using hardware-in-the-loop simulation. Vehicle System Dynamics 1997; 27 (5-6): 423-434. doi: 10.1080/00423119708969340

[4] Choi SB, Choi YT, Park DW. A sliding mode control of a full-car electrorheological suspension system via hardware in-the-loop simulation. Journal of Dynamic Systems, Measurement, and Control 2000; 122 (1): 114-121. doi: 10.1115/1.482435

[5] Lee HS, Choi SB. Control and response characteristics of a magneto-rheological fluid damper for passenger vehicles. Journal of Intelligent Material Systems and Structures 2000; 11 (1): 80-87. doi: 10.1106/412A-2GMA-BTUL-MALT

[6] Choi SB, Lee HS, Park YP. H∞ control performance of a full-vehicle suspension featuring magnetorheological dampers. Vehicle System Dynamics 2002; 38 (5): 341-360. doi: 10.1076/vesd.38.5.341.8283

[7] Choi SB, Seong MS, Ha SH. Vibration control of an MR vehicle suspension system considering both hysteretic behavior and parameter variation. Smart Materials and Structures 2009; 18 (12): 125010. doi: 10.1088/0964-1726/18/12/125010

[8] Hong KS, Sohn HC, Hedrick JK. Modified skyhook control of semi-active suspensions: A new model, gain scheduling, and hardware-in-the-loop tuning. The Journal of Dynamic Systems, Measurement, and Control 2002; 124 (1): 158-167. doi: 10.1115/1.1434265

[9] Batterbee DC, Sims ND. Hardware-in-the-loop simulation of magnetorheological dampers for vehicle suspension systems. Proceedings of the Institution of Mechanical Engineers Part I, Journal of Systems and Control Engineering 2007; 221 (I2): 265-278. doi: 10.1243/09596518JSCE304

[10] Metered H, Bonello P, Oyadiji SO. An investigation into the use of neural networks for the semi-active control of a magnetorheologically damped vehicle suspension. Proceedings of the Institution of Mechanical Engineers Part D Journal of Automobile Engineering 2010; 224 (D7): 829-848. doi: 10.1243/09544070JAUTO1481

[11] Tudon MJC, Jesus LSJ, Morales MR, Ramirez MR, Sename O et al. Hardware-in-the-loop testing of on-off controllers in semi-active suspension systems. In: The 13th Mini Conference on Vehicle System Dynamics Identification and Anomalies (VSDIA); Budapest, Hungary; 2012. pp. 531-53.

[12] Yıldız AS, Sivrioğlu S, Zergeroğlu E, Çetin S. Nonlinear adaptive control of semi-active MR damper suspension with uncertainties in model parameters. Nonlinear Dynamics 2015; 79 (4): 2753-2766. doi: 10.1007/s11071-014-1844-9

[13] Pang H, Chen JN. Adaptive backstepping tracking control for vehicle semi-active suspension system with magnetorheological damper. Binggong Xuebao/Acta Armamentarii 2017; 38 (7): 1430-1442. doi: 10.3969/j.issn.1000-1093.2017.07.023

[14] Song X, Ahmadian M, Southward S, Miller LR. An adaptive semi-active control algorithm for magnetorheological suspension systems. Journal of Vibration and Acoustics 2005; 127 (5): 493-502. doi: 10.1115/1.2013295

[15] Huang Y, Na J, Wu X, Gao GB, Guo Y. Robust adaptive control for vehicle active suspension systems with uncertain dynamics. Transactions of the Institute of Measurement and Control 2018; 40 (4): 1237-1249. doi: 10.1177/0142331216678312

[16] Madura VK, Kodavanla B, Srinivasa R, Madhavi V. Design and experimental study of semi active system of MR damper for vibration control. International Journal of Mechanical and Production Engineering Research and Development 2018; 8 (5): 125-132.

[17] Cetin S, Sivrioglu S, Zergeroğlu E, Yüksek I. Semi-active $H\infty$ robust control of six degree of freedom structural system using MR damper. Turkish Journal of Electrical Engineering & Computer Sciences 2011; 19 (5): 797-805. doi: 10.3906/elk-1007-587

[18] Spencer JB, Dyke S, Sain M, Carlson J. Phenomenological model for magnetorheological dampers. Journal of Engineering Mechanics 1997; 123 (3): 230-238. doi: 10.1061/(ASCE)0733-9399(1997)123:3(230)

[19] Sakai C, Ohmori H, Sano A. Modeling of MR damper with hysteresis for adaptive vibration control. In: International Conference on Decision and Control; Maui, HI, USA; 2003. pp. 3840-3845. doi: 10.1109/CDC.2003.1271748

[20] Yildiz AS, Sivrioglu S, Zergeroglu E, Cetin S. Adaptive control of semiactive quarter car model with MR damper. In: The 9th Asian Control Conference (ASCC); Istanbul, Turkey; 2013. pp. 1-6. doi: 10.1109/ASCC.2013.6606324

[21] Yang ZY, Liang S, Sun YS, Zhu Q. Vibration suppression of four degree-of-freedom nonlinear vehicle suspension model excited by the consecutive speed humps. Journal of Vibration and Control 2016; 22 (6): 1560-1567. doi: 10.1177/1077546314543728

[22] Karnopp D, Crosby MJ, Harwood R. Vibration control using semi-active force generators. Journal of Engineering for Industry 1974; 96 (2): 619-626. doi: 10.1115/1.3438373

[23] Agostinacchio M, Ciampa D, Olita S. The vibrations induced by surface irregularities in road pavements–a Matlab® approach. European Transport Research Review 2014; 6 (3): 267-275. doi: 10.1007/s12544-013-0127-8

[24] Altun Y. The road disturbance attenuation for quarter car active suspension system via a new static two-degree-of-freedom design. An International Journal of Optimization and Control: Theories & Applications (IJOCTA) 2017; 7 (2): 142-148. doi: 10.11121/ijocta.01.2017.00458

[25] Altun Y. Çeyrek taşıt aktif süspansiyon sistemi için LQR ve LQI denetleyicilerinin karşılaştırılması. Gazi Üniversitesi Fen Bilimleri Dergisi Part C Tasarım ve Teknoloji 2017; 5 (3): 61-70 (in Turkish with an abstract in English).

[26] Ahmadian M, Song X, Southward SC. No-jerk skyhook control methods for semiactive suspensions. Transactions of the ASME-L-Journal of Vibration and Acoustics 2004; 126 (4): 580-584. doi: 10.1115/1.1805001